Received 15 January 2020; revised 24 February 2020; accepted 4 March 2020. Date of publication 9 March 2020; date of current version 19 March 2020.
The review of this paper was arranged by Editor C. C. McAndrew.

Digital Object Identifier 10.1109/JEDS.2020.2979240

A Compact Model of MoS_2 Field-Effect Transistors From Drift-Diffusion to Ballistic Carrier Transport Regimes

JIAWEI ZENG[1], WANLING DENG[1], CHANGJIAN ZHOU[2], JIE PENG[1], AND JUNKAI HUANG[1]

1 Department of Electronic Engineering, Jinan University, Guangzhou 510630, China
2 School of Microelectronics, South China University of Technology, Guangzhou 510640, China

CORRESPONDING AUTHOR: W. DENG (e-mail: dwanl@126.com)

This work was supported by the Guangdong Natural Science Foundation under Grant 2018A030313018.

ABSTRACT In this letter, a compact model for charge and drain current in molybdenum disulfide (MoS_2) field-effect transistors (FETs) is developed, which is valid from ballistic to quasi-ballistic to drift-diffusion electronic transport regimes. Considering the influence of trap charges in MoS_2 transistors, a physical-based and analytical charge model is derived. Based on the virtual source model which applies to both ballistic and quasi-ballistic transports, the carrier number density and current expressions are combined to yield the current-voltage (I-V) characteristics. Furthermore, the presented model is validated by experimental data as well as recently reported simulations for MoS_2 FETs with different gate lengths. It shows that our model is accurate, straight-forward, scalable and compatible for short- and long-channel devices.

INDEX TERMS Molybdenum disulfide (MoS_2), charge model, current-voltage (I-V) characteristics.

I. INTRODUCTION

Recently, considerable attention has been paid to 2-D layered transition metal dichalcogenide (TMD), for example, the single-atomic-layer molybdenum disulfide (MoS_2) because of its excellent intrinsic carrier transport properties [1] and transistor scalability [2]. Over the past five years, extremely scaled MoS_2 field-effect transistors (FETs) with gate lengths of 1 nm [3] and 7.5 nm [4] have been experimentally realized. In addition, relevant simulation devices at the scale of sub-5-nm gate length were assessed by solving nonequilibrium Green's function (NEGF) transport equation self-consistently with Poisson's equation [5]. To project the ultimate scaling limit of monolayer MoS_2 transistors, ballistic quantum transport simulations solving by NEGF were performed [1]. The previous researches show that ballistic transport needs to be modeled for MoS_2 transistor if its channel length (L) is smaller than the mean free path (λ), i.e., $L < \lambda$. Besides, some complex digital logic and high-frequency ac applications on MoS_2 FETs such as static random access memories and five-stage ring oscillators have been observed experimentally [6]. Thus, better understanding and modeling of the operation of a 2-D FET are required at the new circuit-level applications.

Several physical-based analytical models [7]–[9] have been proposed for current-voltage (I-V) characteristics of TMD FETs based on the drift-diffusion picture, without applicability to the ballistic and quasi-ballistic regimes [10]–[12]. To perform the ballistic transport effect, some compact models for short-channel devices [10], [11] were proposed but only for the subthreshold region. Furthermore, the work of [12] used an improved method of traditional virtual source (VS) model [13] and made the long-channel device models continue to work well at the nanoscale. However, the charge expression in this model was given by a conventional device equation $Q_{top} = C_{OX}(V_{gs} - V_T)$ where V_T is the threshold voltage, and used a smoothing function to connect different regions. Therefore, it provides a lower physical description.

To this end, in this paper, a physical-based charge expression of MoS_2 FETs is deduced by taking the trap effect into account. Combining with the charge formulation and concerning MoS_2's characteristics, an I-V model is presented

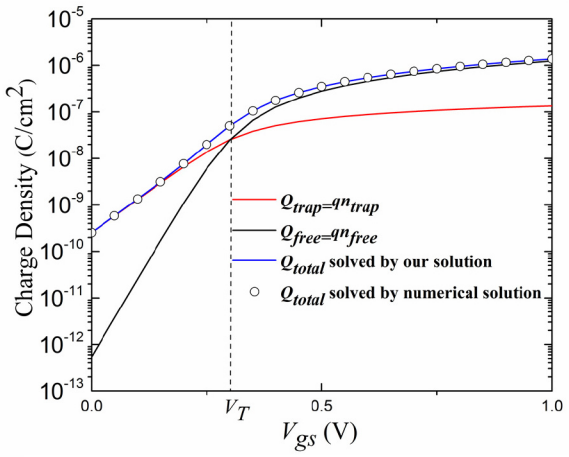

FIGURE 1. The plot of charge density as a function of V_{gs} at the source, where V_T is calculated by the condition $Q_{free} = Q_{trap}$.

which can be applied from drift-diffusion to ballistic carrier transport regimes. Furthermore, the calculated drain current is compared with available simulations and measurements at different channel lengths (1.5 μm, 50 nm and 1 nm) to ensure the model's accuracy and scalability.

II. CHARGE MODEL

For MoS_2 FETs, the density of states (DOS) is represented as a function of the energy E [9]:

$$DOS_{2D}(E) = \begin{cases} D_0 & \text{above } E_C \\ N_T \exp\left(\frac{E-E_C}{k_B T_0}\right) & \text{band tail below } E_C \end{cases} \quad (1)$$

where E_C is the conduction band energy level; N_T [$\text{cm}^{-2}\text{eV}^{-1}$] denotes the total concentration of trap states; k_B is the Boltzmann constant; T_0 is the disorder magnitude parameter; and D_0 [$\text{cm}^{-2}\text{eV}^{-1}$] is the constant DOS. Based on (1) and Fermi-Dirac distribution, after integration, the total carrier number density is given by the sum of the trap (n_{trap}) and free (n_{free}) carrier number densities:

$$\begin{aligned} n_{total} = n_{trap} + n_{free} &= N_T \theta_t \exp\big((\varphi_s + \phi_{f0} - V)/E_1\big) \\ &+ D_0 k_B T \exp\big((\varphi_s + \phi_{f0} - V)/\phi_{th}\big) \end{aligned} \quad (2)$$

where $\theta_t = \pi k_B T / \sin(\pi T/T_0)$; $E_1 = k_B T_0/q$; φ_s is the surface potential; ϕ_{th} is the thermal voltage; V is the quasi-Fermi potential; and ϕ_{f0} is the potential gap between E_C and the neutral Fermi level. Furthermore, using the property of Gauss's law [14], the charge density (Q_{total}) can be calculated by the implicit relation between the applied gate voltage (V_{gs}) and surface potential:

$$Q_{total} = C_{OX}\big(V_{gf} - \varphi_s\big) = q\big(n_{trap} + n_{free}\big) \quad (3)$$

where $V_{gf} = V_{gs} - V_{fb}$; V_{fb} is the flat-band voltage; and C_{OX} is the unit-area gate oxide capacitance. To obtain Q_{total}, an explicit approximation of φ_s is needed. Consequently, the regional approach is adopted here to derive the asymptotic solutions.

TABLE 1. Parameters used for simulations in Fig. 1.

Parameter	Value	Parameter	Value
T [K]	300	C_{OX} [F/cm^2]	2.2×10^{-6}
V_{fb} [V]	−0.05	D_0 [cm^{-2}eV^{-1}]	1×10^{14}
ϕ_{f0} [V]	−0.4	N_T [cm^{-2}eV^{-1}]	6.3×10^{12}
T_0 [K]	700		

In the subthreshold region, n_{trap} dominates and n_{free} can be ignored, and therefore, the surface potential only accounting for the trap states (j_{sub}) can be derived via the Lambert W function (W_0) [15]:

$$\varphi_{sub} = E_1 \ln\left[W_0\left(\frac{A_0}{E_1}\exp\left(\frac{V_{gf}}{E_1}\right)\right)\left(\frac{E_1}{A_0}\right)\right] \quad (4)$$

where A_0 is $(qN_T\theta_t/C_{OX}) \cdot \exp((\phi_{f0} - V)/E_1)$.

In the above-threshold regime, opposite to the subthreshold region, n_{trap} is negligible and n_{free} becomes the dominant term. Only considering the contribution of free charge in Gauss's law, we obtain the explicit solution of the surface potential in the above-threshold region (j_{ab}) as

$$\varphi_{ab} = \phi_{th} \ln\left[W_0\left(\frac{A_1}{\phi_{th}}\exp\left(\frac{V_{gf}}{\phi_{th}}\right)\right)\left(\frac{\phi_{th}}{A_1}\right)\right] \quad (5)$$

where A_1 is $(q\phi_{th}D_0/C_{OX}) \cdot \exp((\phi_{f0} - V)/\phi_{th})$.

Generally, the formula is required to be completely uniform, continuous and smooth across all regions. In order to do that, a following smooth function [16] can be used to obtain φ_s.

$$\varphi_{s0} = \frac{\varphi_{sub}}{1 + \exp\big(m_1(V_{gs} - V_T)\big)} + \frac{\varphi_{ab}}{1 + \exp\big(m_1(V_T - V_{gs})\big)} \quad (6)$$

where m_1 is a fitting parameter.

With the explicit solution of φ_s, charge calculation in (3) can be obtained. Figure 1 with parameters summarized in Table 1 shows that the values of Q_{trap} are much larger than Q_{free} below V_T, and trap density incorporated in the model also can better capture the real device behavior. On the other hand, Q_{free} is dominated above V_T. The solution of Q_{total} using (3) and (6) is consistent with the numerical results, which also verifies the feasibility of the new charge model.

III. DRAIN CURRENT MODEL DESCRIPTION

For aggressively scaled MoS_2 FETs, to gain a better understanding of this futuristic device and offer early evaluation studies, the improved VS model [12] is employed. Under a small drain-to-source voltage (V_{ds}), the drain current in linear region (I_{ds_lin}) can be demonstrated by:

$$I_{ds\_lin} = \left(\frac{W}{L}\right) Q_{top} \mu_{app} V_{ds} \quad (7)$$

$$\mu_{app} = \left(\mu_B^{-1} + \mu_{eff}^{-1}\right)^{-1} \quad (8)$$

where W and L are channel width and length, respectively.

The inversion charge (Q_{top}) at the top of the barrier between the source and drain can be solved by (3) with

$V = 0$, due to the point at the top of barrier is near or at the source edge of channel [17]. It should be noted that, compared to the traditional charge expression in VS model, Q_{top} as a function of surface potential is single-piece without using smoothing functions. As shown in Fig. 1, the charge density is accurately described, which is exponentially dependent on V_{gs} in the subthreshold region and varies linearly with V_{gs} in the above-threshold regime. It is clear that this charge model is more straightforward and physics-based.

In Eq. (8), μ_{app} is the apparent mobility [18] whose definition is based on the ballistic transistor theory. μ_{eff} and μ_B are traditional and ballistic mobilities respectively, yielding [19]

$$\mu_B = v_B L/(2\phi_{th}) \tag{9}$$

where v_B (i.e., $v_B = \sqrt{2k_BT/\pi m^*}$) is the thermal velocity, and m^* is the effective mass of MoS_2.

For long-channel MoS_2 FETs, conduction mechanism is variable-range hopping, and therefore, similar to [9], the effective mobility μ_{eff} is written as

$$\mu_{eff} = \mu_0 + \mu_{hop} \exp\left(\frac{\varphi_s - \varphi_{st} - (E_{tr}/q)}{\phi_{th}}\right) \tag{10}$$

where μ_0 is the channel mobility in the subthreshold region, μ_{hop} is the hopping mobility, and E_{tr} is the effective transport energy most visited by charge carrier via localized states [9]. Herein, φ_{st} is the surface potential in (3) corresponding to $V_{gs} = V_T$. As a result, we can obtain:

$$\varphi_{st} = -\phi_{f0} + \phi_{th} \ln\left[\left(\frac{D_0 k_B T}{N_T \theta_t}\right)^{\frac{T_0}{T-T_0}}\right]. \tag{11}$$

It is not difficult to find that below V_T, μ_0 dominates and above V_T, the exponential term in (10) becomes the dominant term.

According to (8), μ_{app} is the smaller part of μ_{eff} and μ_B. Since μ_B is proportional to the channel length, μ_{app} is close to μ_{eff} at long-channel devices and approaches μ_B at short-channel devices.

Under a high V_{ds}, the drain current in saturation (I_{ds_sat}) becomes:

$$I_{ds\_sat} = WQ_{top}v_{inj} \tag{12}$$

$$v_{inj} = \left(v_B^{-1} + \left(\frac{D_n}{l}\right)^{-1}\right)^{-1} \tag{13}$$

where v_{inj} is the injection velocity which is defined as the mean velocity of carriers at the bottleneck point [17]. D_n (i.e., $D_n = \mu_{eff}\phi_{th}$) and l are the diffusion coefficient and critical length where an electron scattering in this regime has a chance to return to the source. According to [20], l is semi-empirically given by

$$l = L(1 - f_2) + \xi L f_2 \tag{14}$$

$$f_2 = \frac{V_{ds}/(\theta\phi_{th})}{\left[1 + (V_{ds}/(\theta\phi_{th}))^{\beta}\right]^{1/\beta}} \tag{15}$$

where ξ is the ratio of l in saturation and L, which is a fitting parameter from calibration with experimental data. Parameters θ and β are universally fitted which describe the sharpness of the transition of l from L (linear region) to ξL (saturation region).

Similarly, Eq. (13) shows the injection velocity is the smaller part of the velocity at which electrons diffuse across the critical region (D_n/l) and the velocity v_B at which electrons are thermionically emitted across the barrier into the channel. When the critical length is extremely short, the injection velocity reaches v_B.

To acquire the full range of *I-V* characteristics, an empirical function F_{sat} (V_{ds}) is presented like VS model, so the new *I-V* model can be expressed as

$$I_{ds0} = WQ_{top}v_{inj}F_{sat} \tag{16}$$

$$F_{sat} = \frac{V_{ds}/V_{dsat}}{\left(1 + (V_{ds}/V_{dsat})^{\beta}\right)^{\frac{1}{\beta}}} \tag{17}$$

where $V_{dsat} = \alpha L v_{inj}/\mu_{app}$; and α is a saturation-transition-region fitting parameter.

Although the new *I-V* model is similar to the VS model in form, the detailed physical meanings contained in μ_{app} and v_{inj} are the major improvements.

The drain induced barrier lowering effect (DIBL) can significantly affect the subthreshold characteristics. To reflect this effect, in surface potential calculation, we replace V_{gf} by an effect gate voltage (V_{gf}-σV_{ds}) [16], where s is a fitting parameter dependent on channel length.

Furthermore, considering the influence of non-saturation characteristics [21], the drain current becomes $I_{ds} = (1 + MV_{deff})I_{ds0}$, where M is a fitting parameter, and $V_{deff} = V_{ds} - (\varphi_{sd} - \varphi_{ss})$ with φ_{ss} and φ_{sd} as the surface potentials in the source and drain ends, respectively.

Meantime, for MoS_2 transistors, due to the formation of interfacial Schottky barriers at metal/semiconductor interfaces, the efficient carrier transfer is blocked [22]. Therefore, contact resistance is an inevitable problem in the *I-V* modelling of MoS_2 FETs. In our work, similar to [23], the expression for the contact resistances of Schottky barriers which is V_{gs} dependent, can be empirically modelled:

$$R_{contact} = R_m + R_0 \exp\left(-\frac{q}{k_BT}(\Delta_1 V_{gs})\right) \tag{18}$$

where R_0 and R_m are the contact resistances under low and high voltage biases, respectively. Δ_1 is voltage coupling coefficient used as a fitting parameter here. Therefore, to account for the voltage drop on contact resistance, we replace V_{gs} and V_{ds} with V_{gsi} and V_{dsi} in the *I-V* model where $V_{gsi} = V_{gs} - \frac{1}{2}I_{ds}R_{contact}$ and $V_{dsi} = V_{ds} - I_{ds}R_{contact}$. The value of corrected current can be obtained in the iterative way.

All in all, the above *I-V* model applies to single-gate transistors. If the devices are symmetric double-gate transistors, we can get a similar equation like single-gate transistors by rewriting the relation between surface potential and Gauss's

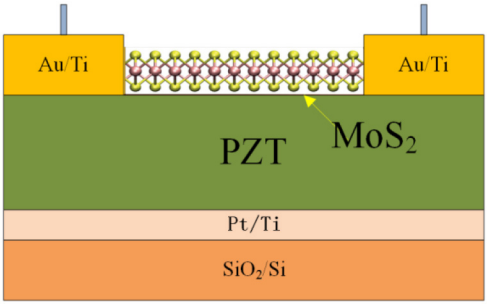

FIGURE 2. Schematic representation of the PZT gated MoS_2 transistor with a 1.5μm channel length and 20μm nominal channel width.

law [8] as:

$$\begin{aligned} Q_{total} &= C_{OX}\left(V_{fg} - V_{ffb} - \varphi_s\right) + C_{BOX}\left(V_{bg} - V_{bfb} - \varphi_s\right) \\ &= C_{OX}\left(V_{geff} - \Psi\varphi_s\right) \\ &= q\left[N_T\theta_t \exp\left(\frac{\varphi_s + \phi_{f0} - V}{E_1}\right)\right. \\ &\quad \left. + D_0 k_B T \exp\left(\frac{\varphi_s + \phi_{f0} - V}{\phi_{th}}\right)\right] \end{aligned} \tag{19}$$

where

$$V_{geff} = V_{fg} + \frac{C_{BOX}}{C_{OX}}V_{bg} - V_{to}, \text{ and } \Psi = 1 + \frac{C_{BOX}}{C_{OX}}.$$

In (19), $V_{to} = V_{ffb} + (C_{OX}/C_{BOX})V_{bfb}$; $V_{f/b,g}$ are the front- and back-gate voltages; $V_{f/b,fb}$ are the flat-band voltages corresponding to the front/back gate; C_{OX} and C_{BOX} are the front- and back-gate-oxide capacitances, respectively. Therefore, the charge/current model of single-gate transistors can be used in symmetric double-gate transistors after V_{gf} is changed into V_{geff} and φ_s in RHS of (3) into $\alpha\varphi_s$.

IV. RESULT AND DISCUSSION

To obtain experimental data, PZT ($pb(Zr_{0.52}Ti_{0.48})O_3$) gated MoS_2 transistors were fabricated [24]. As shown in Fig. 2, on a 300nm SiO_2/Si wafer, a layer of Pt/Ti (100nm/10nm) was sputtered as the bottom gate material and also the seed layer for PZT deposition. Afterwards by a radio frequency sputtering method using a ceramic target, the ultra high-k gate dielectric PZT was prepared (the PZT dielectric is calculated to be in the range of 250-350). The source and the drain locate the top side and channel material is a CVD synthesized MoS_2 atomic layer.

The proposed *I-V* model comparison with the experiment data for the long channel device ($L = 1.5$ μm) is shown in Fig. 3. The values of D_0 and N_t come from the reported literature for experimental MoS_2 transistors [25], [26]. Compared with mean free path λ of MoS_2 (~15 nm), the transport of this device belongs to the drift-diffusion model. In addition, the values of (D_n/l) and μ_{eff} are respectively obtained as 1.6×10^3 cm/s and ~1 $cm^2/(V{\cdot}s)$ in saturation, which are much lower than μ_B and v_B from (9). Consequently, (D_n/l) and μ_{eff} dominate v_{inj} and μ_{app} respectively, which also prove that the transport model is

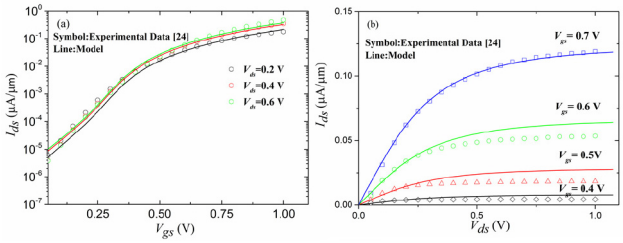

FIGURE 3. Comparisons of (a) transfer and (b) output characteristics for the device with $L = 1.5\mu$m.

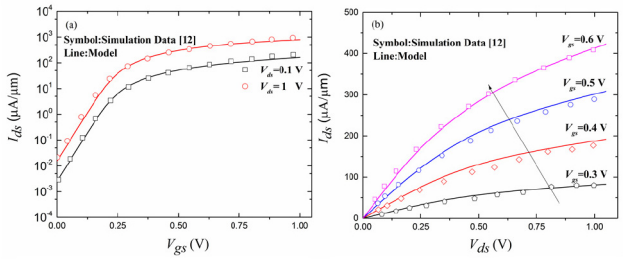

FIGURE 4. Comparisons of (a) transfer and (b) output characteristics for the device with $L = 50$nm.

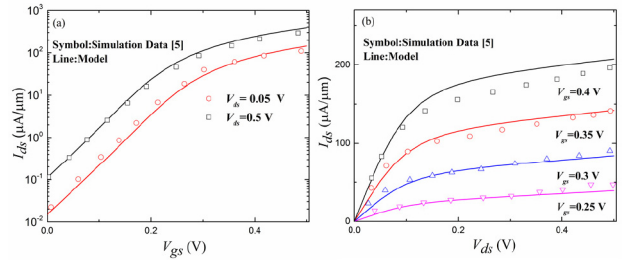

FIGURE 5. Comparisons of (a) transfer and (b) output characteristics for a symmetric double-gate device with $L = 1$nm.

drift-diffusion. Based on the experiments in [23] and [27], it is found that R_0 varies from $10^5\Omega\mu$m to $10^6\Omega\mu$m, and R_m changes from $10^3\Omega\mu$m to $10^4\Omega\mu$m for Ti/Au contact MoS_2 devices. In the sample of Fig. 3 which also uses Ti/Au contact, $R_0 = 1 \times 10^5$ $\Omega\mu$m and $R_m = 1 \times 10^3$ $\Omega\mu$m are used. Good agreements of model and experiment data show that our improved model based on VS model can work well at the microscale.

Moreover, MoS_2 transistors in Figs. 4 and 5 are nano devices with L_g of 50 and 1 nm, of which the *I-V* characteristics are assessed by Monte Carlo simulation and NEGF transport equation self-consistently with the Poisson's equation, respectively. Since the channel lengths are close to or even smaller than λ of MoS_2, quasi-ballistic/ballistic transport should be taken into account. Similar to the previous discussion, we find that v_B and μ_B gradually become the dominant components of v_{inj} and μ_{app}. The transport form is shifted from drift-diffusion to quasi-ballistic/ballistic transport. Because simulation data in Figs. 4 and 5 was computed from Monte Carlo or NEGF, the contact resistance is not considered in our model.

All parameters are given in Table 2 for three groups of *I-V* data. Corresponding to the 1.5 μm, 50 nm, 1 nm devices

TABLE 2. Parameters used for simulations in Figs. 3-5.

Symbol (unit)	Value in Fig.3	Value in Fig.4	Value in Fig.5
C_{OX}(F/cm^2)	2.2×10^{-6}	1.75×10^{-6}	1.18×10^{-6}
ϕ_{f0} (V)	−0.4	−0.4	−0.47
D_0 (cm^{-2}eV^{-1})	1×10^{14}	1×10^{14}	1×10^{14}
N_T (cm^{-2}eV^{-1})	6.3×10^{12}	1×10^{13}	1×10^{13}
T_0 (K)	700	350	450
V_{fb} (V)	−0.05	−0.1	−0.15
α (-)	1.2	4	2
ξ (-)	1/10	1/15	1/15
β (-)	2	2.5	2.5

in Figs. 3-5, the values of injection velocity are obtained as 1.6×10^3, 5.9×10^6 and 7.1×10^6 cm/s, respectively. As the channel length decreases, the trend that the injection velocity reaches its ballistic limit v_B clearly exits. Although this new *I-V* model is similar to the VS model, the physical meanings of μ_{app} and v_{inj} are explained clearly.

V. CONCLUSION

In this paper, the solution of Q_{top} uses a more physical scheme instead of the original semi-empirical method in VS model. Based on this charge expression including the trap effect, a compact model perfectly depicts the *I-V* characteristics of MoS_2 FETs from drift-diffusion to ballistic carrier transport regimes. The good results in Figs. 3-5 show that our works is expected to be useful for MoS_2 devices where extreme scalability is required.

REFERENCES

[1] Y. Yoon, K. Ganapathi, and S. Salahuddin, "How good can monolayer MoS_2 transistors be?" *Nano Lett.*, vol. 11, no. 9, pp. 3768–3773, Jul. 2011, doi: 10.1021/nl2018178.

[2] S. Das, H.-Y. Chen, A. V. Penumatcha, and J. Appenzeller, "High performance multilayer MoS_2 transistors with scandium contacts," *Nano Lett.*, vol. 13, no. 1, pp. 100–105, Jan. 2013, doi: 10.1021/nl303583v.

[3] S. B. Desai *et al.*, "MoS_2 transistors with 1-nanometer gate lengths," *Science*, vol. 354, no. 6308, pp. 99–102, Oct. 2016, doi: 10.1126/science.aah4698.

[4] A. Nourbakhsh *et al.*, "MoS_2 field-effect transistor with sub-10nm channel length," *Nano Lett.*, vol. 16, no. 12, pp. 7798–7806, Dec. 2016, doi: 10.1021/acs.nanolett.6b03999.

[5] Z. Dong and J. Guo, "Assessment of 2-D transition metal dichalcogenide FETs at sub-5-nm gate length scale," *IEEE Trans. Electron Devices*, vol. 64, no. 2, pp. 622–628, Feb. 2017, doi: 10.1109/TED.2016.2644719.

[6] H. Wang *et al.*, "Integrated circuits based on bilayer MoS_2 transistors," *Nano Lett.*, vol. 12, no. 9, pp. 4674–4680, Sep. 2012, doi: 10.1021/nl302015v.

[7] D. Jiménez, "Drift-diffusion model for single layer transition metal dichalcogenide field-effect transistors," *Appl. Phys. Lett.*, vol. 101, no. 24, Dec. 2012, Art. no. 243501, doi: 10.1063/1.4770313.

[8] C. Yadav, A. Agarwal, and Y. S. Chauhan, "Compact modeling of transition metal dichalcogenide based thin body transistors and circuit validation," *IEEE Trans. Electron Devices*, vol. 64, no. 3, pp. 1261–1268, May 2017, doi: 10.1109/TED.2016.2643698.

[9] L. Wang, Y. Li, X. Gong, A. V.-Y. Thean, and G. Liang, "A physics-based compact model for transition-metal dichalcogenides transistors with the band-tail effect," *IEEE Electron Device Lett.*, vol. 39, no. 5, pp. 761–764, May 2018, doi: 10.1109/LED.2018.2820142.

[10] W.-X. You and P. Su, "A compact subthreshold model for short-channel monolayer transition metal dichalcogenide field-effect transistors," *IEEE Trans. Electron Devices*, vol. 63, no. 7, pp. 2971–2974, Jul. 2016, doi: 10.1109/TED.2016.2564424.

[11] M. Gholipour, "A compact short-channel model for symmetric double-gate TMDFET in subthreshold region," *IEEE Trans. Electron Devices*, vol. 64, no. 8, pp. 3466–3469, Aug. 2017, doi: 10.1109/TED.2017.2716951.

[12] T. Wu, X. Cao, and J. Guo, "Compact model of carrier transport in monolayer transition metal dichalcogenide transistors," *IEEE Trans. Electron Devices*, vol. 66, no. 1, pp. 177–183, Jan. 2019, doi: 10.1109/TED.2018.2866095.

[13] A. Khakifirooz, O. M. Nayfeh, and D. Antoniadis, "A simple semiempirical short-channel MOSFET current-voltage model continuous across all regions of operation and employing only physical parameters," *IEEE Trans. Electron Devices*, vol. 56, no. 8, pp. 1674–1680, Aug. 2009, doi: 10.1109/TED.2009.2024022.

[14] Y. Liu, R.-H. Yao, B. Li, and W.-L. Deng, "An analytical model based on surface potential for a-Si:H thin-film transistors," *J. Display Technol.*, vol. 4, no. 2, pp. 180–187, Jun. 2008, doi: 10.1109/JDT.2007.907122.

[15] F. Yu, C. Xu, G. Huang, W. Lin, and T.-C. Liang, "A closed-form trapped-charge-included drain current compact model for amorphous oxide semiconductor thin-film transistors," *Microelectron. Rel.*, vol. 91, pp. 307–312, Dec. 2018.

[16] W. Deng, J. Huang, and X. Li, "Surface-potential-based drain current model of polysilicon TFTs with Gaussian and exponential DOS distribution," *IEEE Trans. Electron Devices*, vol. 59, no. 1, pp. 94–100, Jan. 2012, doi: 10.1109/TED.2011.2172686.

[17] K. Natori, "Ballistic/quasi-ballistic transport in nanoscale transistor," *Appl. Surface Sci.*, vol. 254, no. 19, pp. 6194–6198, Jul. 2008, doi: 10.1016/j.apsusc.2008.02.150.

[18] M. S. Lundstrom and D. A. Antoniadis, "Compact models and the physics of nanoscale FETs," *IEEE Trans. Electron Devices*, vol. 61, no. 2, pp. 225–233, Feb. 2014, doi: 10.1109/ted.2013.2283253.

[19] M. S. Shur, "Low ballistic mobility in submicron HEMTs," *IEEE Electron Device Lett.*, vol. 23, no. 9, pp. 511–513, Sep. 2002, doi: 10.1109/LED.2002.802679.

[20] S. Rakheja, M. S. Lundstrom, and D. A. Antoniadis, "An improved virtual-source-based transport model for quasi-ballistic transistors—Part I: Capturing effects of carrier degeneracy, drain-bias dependence of gate capacitance, and nonlinear channel-access resistance," *IEEE Trans. Electron Devices*, vol. 62, no. 9, pp. 2786–2793, Sep. 2015, doi: 10.1109/TED.2015.2457781.

[21] K. Abe *et al.*, "Simple analytical model of on operation of amorphous In-Ga-Zn-O thin-film transistors," *IEEE Trans. Electron Devices*, vol. 58, no. 10, pp. 3463–3471, Oct. 2011, doi: 10.1109/TED.2011.2160981.

[22] S.-L. Li, K. Tsukagoshi, E. Orgiu, and P. Somari, "Charge transport and mobility engineering in two-dimensional transition metal chalcogenide semiconductors," *Chem. Soc. Rev.*, vol. 45, no. 1, pp. 118–151, Jan. 2016, doi: 10.1039/c5cs00517e.

[23] H.-Y. Chang, W. Zhu, and D. Akinwande, "On the mobility and contact resistance evaluation for transistors based on MoS_2 or two-dimensional semiconducting atomic crystals," *Appl. Phys. Lett.*, vol. 104, no. 11, Mar. 2014, Art. no. 113504, doi: 10.1063/1.4868536.

[24] C. Zhou *et al.*, "Low voltage and high ON/OFF ratio field-effect transistors based on CVD MoS_2 and ultra high-k gate dielectric PZT," *Nanoscale*, vol. 7, no. 19, pp. 8695–8700, May 2015, doi: 10.1039/c5nr01072a.

[25] W. Cao, J. Kang, W. Liu, and K. Banerjee, "A compact current-voltage model for 2D semiconductor based field-effect transistors considering interface traps, mobility degradation, and inefficient doping effect," *IEEE Trans. Electron Devices*, vol. 61, no. 12, pp. 4282–4290, Dec. 2014, doi: 10.1109/TED.2014.2365028.

[26] J. Cao *et al.*, "A new velocity saturation model of MoS_2 field effect transistors," *IEEE Electron Device Lett.*, vol. 39, no. 6, pp. 893–896, Jun. 2018, doi: 10.1109/LED.2018.2830400.
[27] H. Liu *et al.*, "Switching mechanism in single-layer molybdenum disulfide transistors: An insight into current flow across schottky barriers," *Acs Nano*, vol. 8, no. 1, pp. 1031–1038, Jan. 2014, doi: 10.1021/nn405916t.

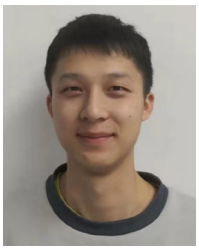

JIAWEI ZENG received the B.S. degree from the Jiangxi University of Science and Technology, Ganzhou, China, in 2018. He is currently pursuing the M.S. degree with Jinan University, Guangzhou.

His current research interest includes the modeling of the MoS_2 transistors.

WANLING DENG received the B.S. and Ph.D. degrees in electrical engineering from the South China University of Technology, Guangzhou, China, in 2003 and 2008, respectively.

Since 2008, she has been an Associate Professor with the Department of ElectronicEngineering, Jinan University, Guangzhou. Her current research interests include thin-film transistor (TFT) devices and physics, particularly poly-Si TFT and AOS TFT modeling.

CHANGJIAN ZHOU received the B.S. degree from Xidian University in 2007, and the Ph.D. degree from Tsinghua University in 2012.

He is currently an Associate Professor with the South China University of Technology. His research interests span across electron devices integrating functional materials and low-dimensional materials, piezoelectronics, micro/nano-electro-mechanical systems, and nanocarbon interconnects.

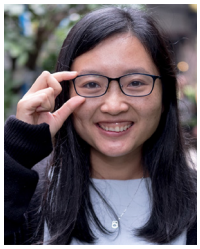

JIE PENG received the B.S. degree in physics from South China Normal University in 2002, and the Ph.D. degree in theorectical physics from Sun Yat-sen University in 2007.

She is currently working as a Lecturer with the Electronic Engineering Department, Jinan University. Her current research interests include electronic transport, photoluminescent of carbon, and semiconductor quantum dots.

JUNKAI HUANG received the B.S. degree in applied physics and the M.S. degree in semiconductor device from Jinan University, Guangzhou, China, in 1985 and 1990, respectively, and the Ph.D. degree from the Institute of Microelectronics, South China University of Technology, Guangzhou, in 2011.

He is currently a Professor with Jinan University. His current research interests include thin-film transistors' modeling, simulation, and integrated circuit design.